Available online at www.derpharmachemica.com

Scholars Research Library

Der Pharma Chemica, 2014, 6(3):64-77
(http://derpharmachemica.com/archive.html)

ISSN 0975-413X
CODEN (USA): PCHHAX

Toward understanding the inhibition of vesicular stomatitis virus replication in MDCK cells by 4-quinolinecarboxylic acid analogues: A density functional study

Juan S. Gómez-Jeria

Quantum Pharmacology Unit, Department of Chemistry, Faculty of Sciences, University of Chile. Las Palmeras, Santiago, Chile

---

ABSTRACT

This paper presents and discusses the relationship between electronic structure and the inhibition capacity of vesicular stomatitis virus (VSV) replication in MDCK cells of a group of 4-quinolinecarboxylic acid analogues. The electronic structure of all molecules was calculated within Density Functional Theory at the B3LYP/6-31g(d,p) level after full geometry optimization. No statistically significant equation was obtained for the whole set. Guessing that some molecules could interact with an extra site, we generate two subsets. For both of them we obtained statistically significant equations relating the variation of the VSV replication inhibitory capacity with the variation of a definite set of local atomic reactivity indices. The process is charge-controlled. The common skeleton hypothesis seems to work well enough.

INTRODUCTION

The vesicular stomatitis virus (VSV) is a member of the *Vesiculovirus* genus, of the *Rhabdoviridae* family. This is a bullet-shaped, enveloped virus, about 170 nm in length and 70 nm in diameter, possessing a single-stranded and negative-sense RNA genome [1-23]. VSV is the causative agent of vesicular stomatitis, a disease of cattle, horses, mules, deer, grasshoppers, rodents, pigs, and occasionally humans [24-33]. Indications of exposure have been found in many species such as antelopes, bats, birds, dogs, cervids and nonhuman primates. However, VSV is also a promising agent for oncolytic virus therapy, an anti-cancer approach employing viruses to preferentially infect and kill cancer cells, while keeping healthy cells intact [34-39]. It is thought that the antiviral responses induced by type I interferon pathways are impaired in a good number of cancer cells. Consequently, cancer cells are more susceptible to VSV than normal ones. Other factors making VSV a promising oncolytic virus candidate for clinical use are the lack of pre-existing immunity in humans, an easily modifiable genome, a relative independence from receptor type or cell cycle, and cytoplasmic replication without the peril of host-cell transformation. There are two possible ways of neutralizing this virus. The first is employing synthetic ligands that bind to key structures of the virus preventing its replication. On the other hand, many viruses employ the host cell machinery to replicate and to avoid the host's immune response. This is the basis for the second approach, which consists in locating and blocking a key structure inside the host that is necessary for viral replication. In the case of VSV, the inhibition of human dihydroorotate dehydrogenase (DHODH), a fundamental enzyme in the *de novo* biosynthesis pathway of pyrimidines, has proved to be an excellent tool for impairing VSV replication. Brequinar and a series of other compounds are products of this approach. Recently, de Brabander et al. synthesized a group of 4-quinolinecarboxylic acid analogues that inhibit

DHODH. They also tested the ability of these compounds to inhibit *in vitro* VSV replication in MDCK (Madin-Darby canine kidney) epithelial cells [40]. To date there are no formal quantitative structure-activity relationships studies dealing with the inhibition of VSV replication. Here we present the results of a quantum-chemical analysis of the relationships between the electronic structure and the *in vitro* anti-VSV replication activity of the abovementioned molecules.

MODELS, METHODS AND CALCULATIONS

The method

Considering that the model-based method [41] employed here has been described and discussed in great detail elsewhere [42-47], we present only a short standard summary. The inhibitory replication, expressed as EC_{50}, is a linear function of several local atomic reactivity indices (LARIs) and has the form:

$$\log(EC_{50}) = a + bM_{D_i} + c\log\left[\sigma_{D_i} / (ABC)^{1/2}\right] + \sum_j \left[e_j Q_j + f_j S_j^E + s_j S_j^N\right] +$$
$$+ \sum_j \sum_m \left[h_j(m) F_j(m) + x_j(m) S_j^E(m)\right] + \sum_j \sum_{m'} \left[r_j(m') F_j(m') + t_j(m') S_j^N(m')\right] +$$
$$+ \sum_j \left[g_j \mu_j + k_j \eta_j + o_j \omega_j + z_j \varsigma_j + w_j Q_j^{\max}\right] + \sum_{B=1}^{W} O_B \qquad (1)$$

where ABC the product of the drug's moment of inertia about the three principal axes of rotation, M is the drug's mass and σ its symmetry number. The nomenclature used below is the following. $HOMO_j$* refers to the highest occupied molecular orbital localized on atom j and $LUMO_j$* to the lowest empty MO localized on atom j. They are the local atomic frontier MOs. The molecule's MOs do not carry an asterisk. Table 1 presents, in the standard form used in other publications, the physical interpretation and units of the LARIs, together with references corresponding to their first historical use [47-49].

Table 1. LARIs and their physical meaning

LARI	Name	Physical interpretation	Units
Q_i	Net atomic charge of atom i	Electrostatic interaction [48]	e
S_i^E	Total atomic electrophilic superdelocalizability of atom i	Total atomic electron-donating capacity of atom i (MO-MO interaction) [49]	e/eV
S_i^N	Total atomic nucleophilic superdelocalizability of atom i	Total atomic electron-accepting capacity of atom i (MO-MO interaction) [49]	e/eV
$S_i^E(m)$	Orbital atomic electrophilic superdelocalizability of atom i and occupied MO m	Electron-donating capacity of atom i at occupied MO m (MO-MO interaction) [49]	e/eV
$S_i^N(m')$	Orbital atomic nucleophilic superdelocalizability of atom i and empty MO m'	Electron-accepting capacity of atom i at vacant MO m' (MO-MO interaction) [49]	e/eV
F_i	Fukui index of atom i	Total electron population of atom I (MO-MO interaction) [49]	e
F_{mi}	Fukui index of atom i and occupied MO m.	Electron population of occupied m MO at atom I (MO-MO interaction) [49]	e
$F_{m'i}$	Fukui index of atom i and empty MO m'	Electron population of vacant MO m' at atom i (MO-MO interaction) [49]	e
μ_i	Local atomic electronic chemical potential of atom i	Propensity of atom i to gain or lose electrons. $HOMO_i$*-$LUMO_i$* midpoint [47]	eV
η_i	Local atomic hardness of atom i	Resistance of atom i to exchange electrons with the environment [47] $HOMO_i$*-$LUMO_i$* gap	eV
ς_i	Local atomic softness of atom i	The inverse of η_i [47]	1/eV
ω_i	Local atomic electrophilicity of atom i	Tendency of atom i to receive extra electronic charge together with its resistance to exchange charge with the medium	eV
$Q_i^{\max}$	Local atomic charge capacity	Maximal amount of electronic charge atom i may receive [47]	---
O_t	Orientational Parameter of the substituent	Influences the fraction of molecules attaining the correct orientation to interact with a partner [44, 45]	uma·Å^2

The application of this method has proved successful for a large number of systems [44, 50-77]. It is important to mention that this method works effectively if and only if all the molecules of the set studied exert their final biological activity through the same mechanism or mechanisms. If this condition is not fulfilled, we cannot expect to obtain the best results for the whole set and must consider other possibilities.

Selection of the experimental data

An essential condition to utilize a set of experimental values in QSAR studies is that they must be obtained under more or less identical experimental conditions and procedures. The biological activity selected for this study is the inhibition of VSV replication (EC_{50}), in MBDK cells [40]. It is worth mentioning that the exact *in vitro* inhibitory mechanism of these molecules is uncertain. The molecules chosen for this study are shown in Figs. 1 and 2, and Tables 2 and 3, together with the corresponding experimental biological activities (see Results, below).

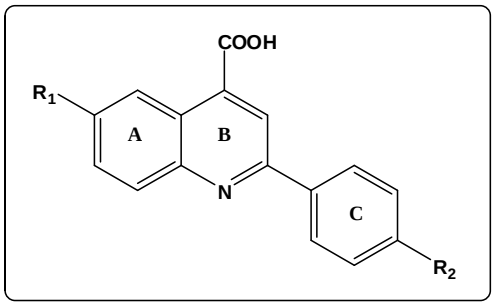

Figure 1. General formula for group A of 4-quinolinecarboxylic acid analogues

Table 2. Group A of molecules and their biological activity

Molecule	R_1	R_2	$\log(EC_{50})$ (μM)
1	Cl	$O(CH_2)_2CH_3$	0.67
2	Cl	OCH_3	0.85
3	Cl	OCH_2CH_3	0.76
4	Cl	$O(CH_2)_3CH_3$	0.81
5	Cl	OCF_3	-0.3
6	Cl	F	0.26
7	Cl	Br	0.34
8	Cl	CH_3	0.94
9	Cl	CH_2CH_3	0.76
10	Cl	CF_3	1.55
11	F	OCH_3	0.81
12	F	OCH_2CH_3	-0.22
13	F	$O(CH_2)_2CH_3$	1.3
14	F	$O(CH_2)_3CH_3$	0.32
15	F	$CH_2(C_3H_5)$	0.83
16	F	CF_3	0

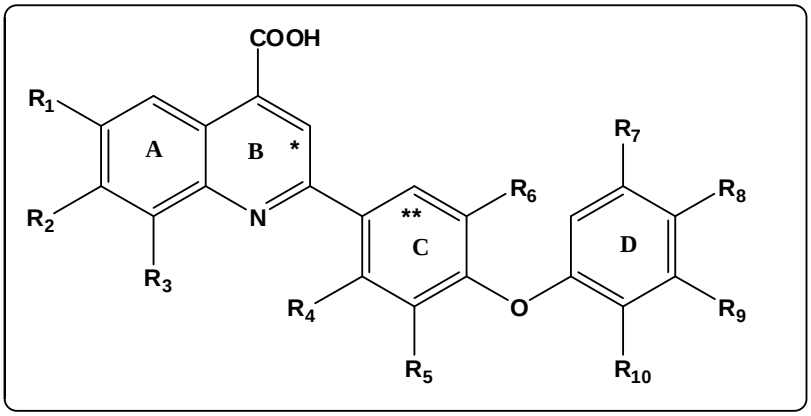

Figure 2. General formula for group B of 4-quinolinecarboxylic acid analogues[a]

Table 3. Group B of molecules and their biological activity

Molecule	R_1	R_6	R_7	R_8	R_9	R_{10}	R_2-R_5	log(EC_{50}) μM
17	H	H	H	H	H	H		0.11
18	F	H	H	H	H	H		-1.00
19	Br	H	H	H	H	H		0.49
20	OCF3	H	H	H	H	H		1.98
21	OCH3	H	H	H	H	H		3.42
22	NO2	H	H	H	H	H		0.30
23	CF3	H	H	H	H	H		1.22
24	H	H	H	H	H	H		0.00
25	H	H	H	H	H	H	R_3=F	0.08
26	H	H	H	H	H	H	R_2=F	2.20
27	F	H	H	H	H	H	R_2=F	0.20
28	F	H	H	H	Cl	H		0.30
20	F	H	H	H	NO_2	H		0.69
30	F	H	H	R_8-R_9(OCH_2O)	------	H		-0.05
31	F	H	F	H	H	H		-0.52
32	F	H	H	F	H	H		-1.00
33	F	H	H	H	F	H		0.00
34	F	H	pyridyl	H	H	H		1.36
35	F	H	H	pyridyl	H	H		0.40
36	F	H	thiazolyl	H	H	H		1.16
37	F	CH_3	H	H	H	H		0.86
38	F	H	H	H	H	H		0.95
39[b]	F	H	H	H	H	H		-0.63
40	F	H	H	CH_3	H	CH3		-0.28
41	F	H	R_7-R_8-C_6H_4	--------	H	H		-0.25
42	F	CH_3	H	H	$C(CH_3)_3$	H		-1.19
43	F	CH_3	H	H	H	H	R_4=CH_3	-1.64
44	F	$CH(CH_3)_2$	H	H	H	H	R_5=CH_3	-2.70

*a. R_2=R_3=R_4=R_5=H in all cases but those mentioned in the last column. b. Atoms marked * and ** are linked by a CH_2 group in Fig. 2. b. This molecule has an extra methylene group linking the O atom and D ring.*

Calculations

The electronic structure of the molecules was obtained within the Density Functional Theory at the B3LYP/6-31g(d,p) level of theory. The Gaussian suite of programs was employed [78]. After full geometry optimization and single point calculations, the values of the LARIs were calculated with D-CENT-QSAR [79]. Electron populations arising from Mulliken Population Analysis were corrected as suggested [80]. Orientational parameters were calculated as usual [44, 45]. As the resolution of the system of linear equations is not achievable because there are not enough molecules, we used Linear Multiple Regression Analysis (LMRA) to find out which atoms are directly involved in the variation of the biological activity. We worked within the hypothesis that there is a set of atoms common to all the molecules studied (called the common skeleton), encoding the variation of the biological activity through the series. It is the variation of the values of some local atomic reactivity indices of the atoms belonging to this skeleton that accounts for the variation of the inhibition of VSV replication throughout the series analyzed. The substituents modify the electronic structure of the common skeleton and control the precise alignment of the common skeleton with its partner through the orientational parameters. For the LMRA, we built a matrix containing the logarithm of the dependent variable (EC_{50}) and the local atomic reactivity indices of the atoms constituting the common skeleton as independent variables. The Statistica software was used [81]. Note that in this kind of model statistics is employed as a servant and not as a queen. The common skeleton numbering is depicted in Fig. 3.

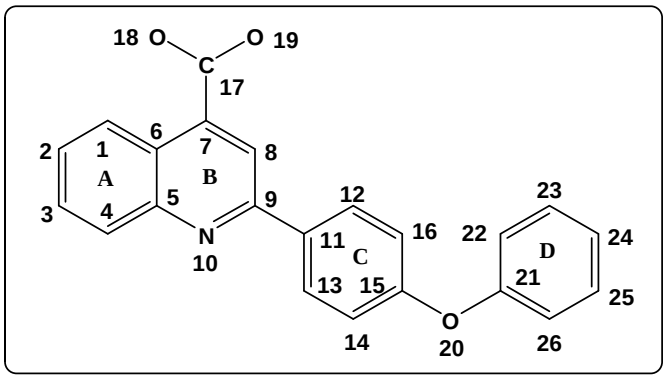

Figure 3. Common skeleton numbering

RESULTS

We carried out a preliminary LMRA with all the molecules (n=44, Tables 2 and 3) using atoms 1-19 as the common skeleton (Fig. 3). No statistically significant results were obtained. On the basis of the observation that several molecules do not have a substituent of the O-phenyl type at R_2 (Fig.1), we formed group A with them (Table 2). The remaining molecules formed group B (molecule 36 was excluded from both groups).

LMRA results for group A of molecules.

For this case, the common skeleton included atoms numbered 1 to 19 in Fig. 3. A first LMRA showed that molecules 12 and 13 were outliers and we discarded them. A second LMRA discarded molecule 14 as an outlier. For the remaining set we obtained the following statistically significant equation:

$$\log(EC_{50}) = -1.16 + 6.97F_3(LUMO+2)^* - 1.22F_{16}(LUMO+1)^* \quad (2)$$

with n=13, R=0.97, R^2=0.95, adj R^2=0.94, F(2,10)=91.02 ($p<0.00001$) and SD=0.12. No outliers were detected and no residuals fall outside the ±2σ limits. Here, $F_3(LUMO+2)^*$ is the Fukui index (the electron population) of the third lowest vacant MO localized on atom 3 and $F_{16}(LUMO+1)^*$ is the Fukui index of the second lowest vacant MO localized on atom 16. The Beta coefficients and t-test for significance of coefficients of Eq. 2 are shown in Table 4. There is no significant internal correlation between the two independent variables (10%). Figure 4 shows the plot of observed values *vs.* predicted ones. The associated statistical parameters of Eq. 2 indicate that this equation is statistically significant, explaining about 94% of the variation of the VSV inhibitory activity.

Table 4: Beta coefficients and *t*-test for significance of the coefficients in Eq. 2

	Beta	t(10)	*p-level*
$F_3(LUMO+2)^*$	0.69	9.11	*<0.000004*
$F_{16}(LUMO+1)^*$	-0.50	-6.52	*<0.00007*

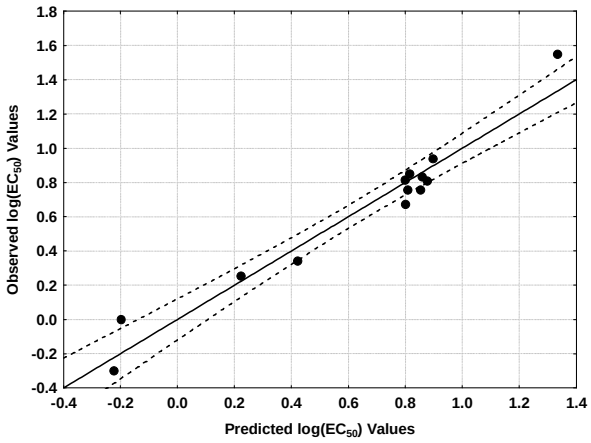

Figure 4: Observed versus predicted values (Eq. 2) of log (EC_{50}). Dashed lines denote the 95% confidence interval

LMRA results for group B of molecules.

For group B the common skeleton included atoms 1-26 of Fig. 1. A series of LMRAs discarded molecules 20, 28, 30, 34-36 and 39 as outliers. For the remaining set we obtained the following statistically significant equation:

$$\log(EC_{50}) = -12.63 - 521.04S_{17}^{E}(HOMO-1)^* - 3.72\mu_{19} - 1.89F_{18}(HOMO-1)^* - \\ -0.16S_{22}^{N}(LUMO+2)^* - 25.13F_{13}(LUMO+1)^* + 16.22F_{19}(LUMO+1)^* - 5.31F_{15}(HOMO-1)^* \quad (3)$$

with n=21, R=0.99, R^2=0.98, adj R^2=0.97, F(7,13)=106.68 ($p<0.00001$) and SD=0.21. No outliers were detected and no residuals fall outside the ±2σ limits. Here, μ_{19} is the local electronic chemical potential of atom 19, $S_{17}^{E}(HOMO-1)*$ is the local atomic electrophilic superdelocalizability of the second highest occupied MO localized on atom 17, $S_{22}^{N}(LUMO+2)*$ is the local atomic nucleophilic superdelocalizability of the third lowest vacant MO localized on atom 22 and, in general, $F_k(MO_z)*$ is the electron population (Fukui index) of MO z localized on atom k. The beta coefficients and t-test for significance of coefficients of Eq. 3 are shown in Table 5. Table 6 shows the squared correlation coefficients for the variables appearing in Eq. 3. No significant internal correlations are observed. Figure 5 shows the plot of observed values *vs.* predicted ones. The associated statistical parameters of Eq. 3 indicate that this equation is statistically significant, explaining about 97% of the variation of the VSV inhibitory activity.

Table 5: Beta coefficients and *t*-test for significance of the coefficients in Eq. 3

	Beta	t(13)	*p-level*
$S_{17}^{E}(HOMO-1)*$	0.86	20.54	*<0.000001*
μ_{19}	-0.61	-15.00	*<0.000001*
$F_{18}(HOMO-1)*$	-0.39	-9.56	*<0.000001*
$S_{22}^{N}(LUMO+2)*$	-0.25	-6.00	*<0.00005*
$F_{13}(LUMO+1)*$	-0.27	-6.36	*<0.00003*
$F_{19}(LUMO+1)*$	0.18	4.68	*<0.0004*
$F_{15}(HOMO-1)*$	-0.12	-3.14	*<0.008*

Table 6: Squared correlation coefficients for the variables appearing in Eq. 3

	$S_{17}^{E}(HOMO-1)*$	μ_{19}	$F_{18}(HOMO-1)*$	$S_{22}^{N}(LUMO+2)*$	$F_{13}(LUMO+1)*$	$F_{19}(LUMO+1)*$
μ_{19}	0.12	1.00				
$F_{18}(HOMO-1)*$	0.005	0.03	1.00			
$S_{22}^{N}(LUMO+2)*$	0.05	0.04	0.13	1.00		
$F_{13}(LUMO+1)*$	0.008	0.0004	0.10	0.02	1.00	
$F_{19}(LUMO+1)*$	0.05	0.02	0.01	0.01	0.06	1.00
$F_{15}(HOMO-1)*$	0.01	0.002	0.03	0.04	0.11	0.07

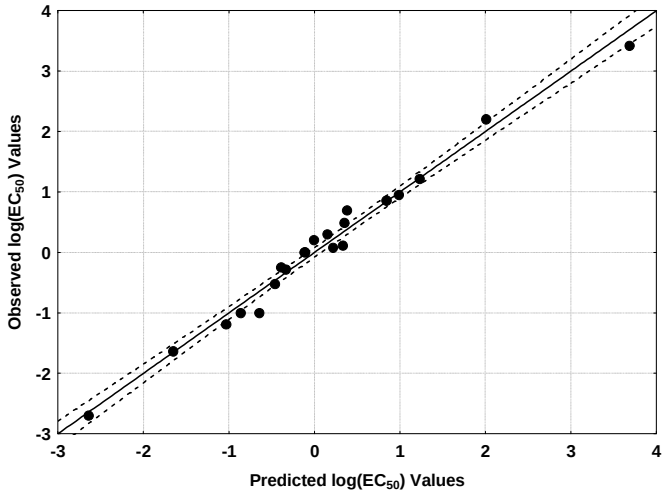

Figure 5: Observed versus predicted values (Eq. 3) of log (EC_{50}). Dashed lines denote the 95% confidence interval

DISCUSSION

If good QSAR results are not obtained, at least two possibilities should be considered. The first is a reformulation of the structure of the common skeleton. The second one is related to the fact that some molecules might exert their biological action via different mechanisms. We have encountered both classes of situations during our research. In the case analyzed here, the hypothesis that a subgroup of molecules interacts with an extra site of the partner led to statistically significant results. As always, there are some variables that do not appear in Eqs. 2 and 3 because their variation is not statistically significant.

Molecular electrostatic potential (MEP) structure.

If groups A and B of molecules exert their inhibitory activities at the same site we expect that their MEP's should be similar for the recognition process. Figs. 6 and 7 display the MEP of molecules 5 and 44, the most active ones of each group [82].

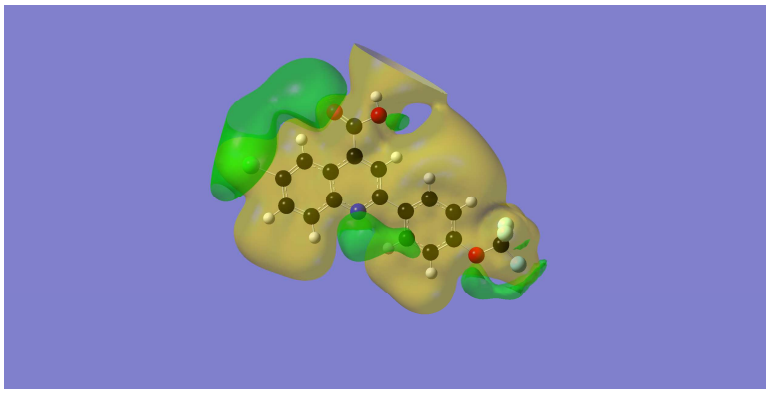

Figure 6. MEP of molecule 5. The green isovalue surface corresponds to negative MEP values (-0.01) and the yellow isovalue surface to positive MEP values (0.01)

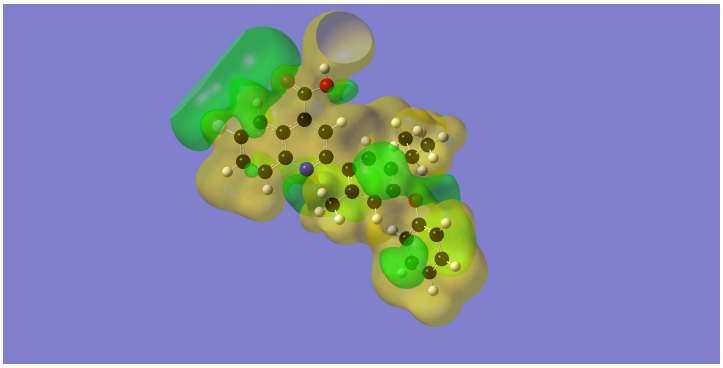

Figure 7. MEP of molecule 44. The green isovalue surface corresponds to negative MEP values (-0.01) and the yellow isovalue surface to positive MEP values (0.01)

We can see that the MEP of both molecules is similar in the region of ring A and the COOH group. The MEP structures of the lower right side are different. Knowing that the COOH substituent is essential for activity, we may guess that the approach of these molecules to their action site and the initial interaction with it is controlled by the MEP around this area. To have an idea of the structure of the MEP at a given distance from the nuclei, we present in Figs. 8 and 9 the MEP of molecules 5 and 44 at a distance of 3.5 Å from the nuclei [83].

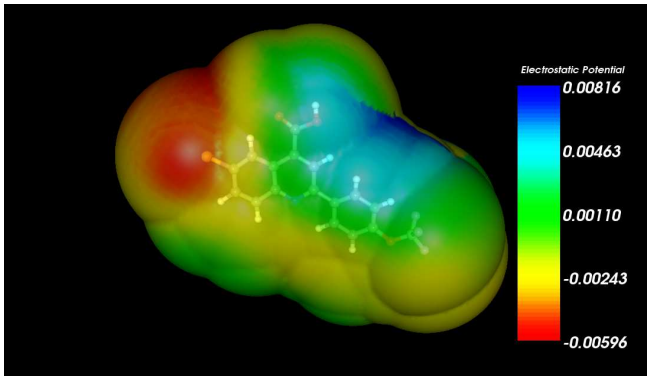

Figure 8. MEP map of molecule 5 at a distance of 3.5 Å from the nuclei

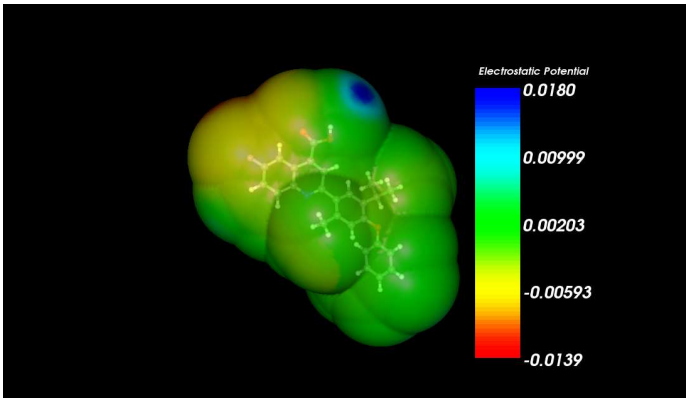

Figure 9. MEP map of molecule 44 at a distance of 3.5 Å from the nuclei

We can see that at 3.5 Å a negative MEP area exists around ring A and the COOH moiety in both molecules. At this distance, the guiding process of the drug molecule towards its partner occurs. In agreement with our previous suggestion we suppose that the guiding and interaction processes takes place with the COOH moiety pointing to its partner.

Structure of the Molecular Orbitals.

Figs. 10 and 11 show, respectively, the HOMO structure and localization of molecules 5 and 44 [82].

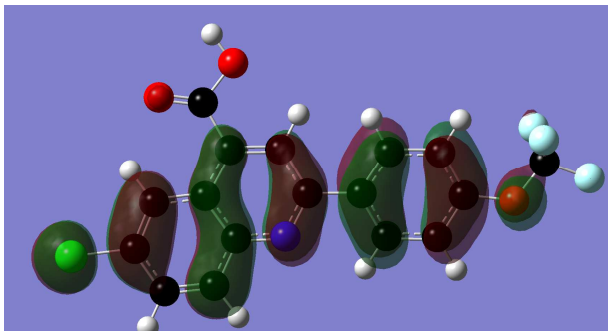

Figure 10. Molecular HOMO of molecule 5 (isovalue=0.02)

We can see that the HOMO is of π nature and is localized on all rings and the Cl substituent (see Figs. 1 and 2). A small localization is observed on the carbonyl oxygen atom of the COOH moiety.

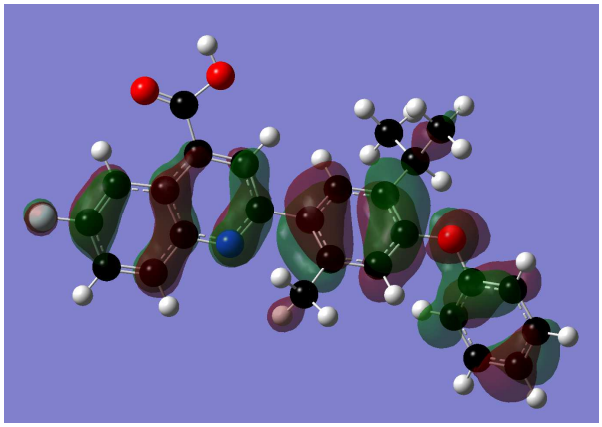

Figure 10. Molecular HOMO of molecule 44 (isovalue 0.02)

We can see that the HOMO is of π nature (with some small σ components) and is localized on all rings. The HOMO structure and localization are similar in both molecules but in molecule 44 the HOMO is also localized on ring D (Fig. 2). No localization is observed on the COOH moiety. Then, if molecule 44 is able to employ ring D to interact as an electron-donor center, it will do so through the molecular HOMO.

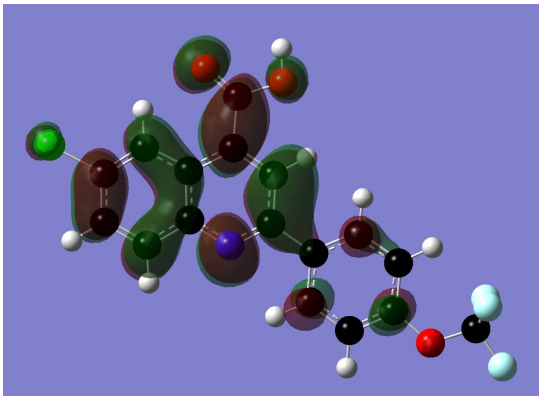

Figure 11. Molecular LUMO of molecule 5 (isovalue=0.02)

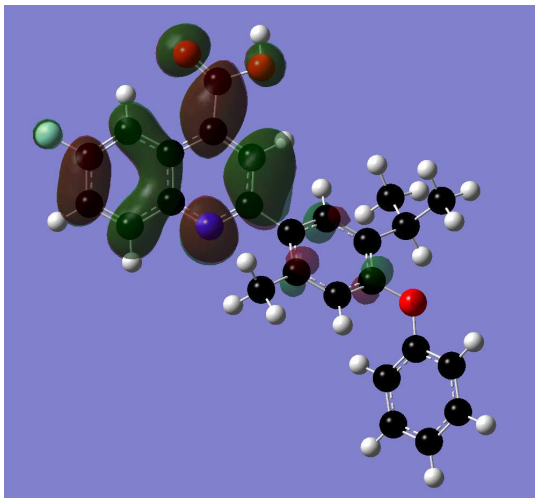

Figure 12. Molecular LUMO of molecule 44 (isovalue=0.02)

We can see that the structure and localization of the LUMO (which is of π nature) are similar in both molecules. In molecule 44 the LUMO is not localized on ring D (Fig. 2). If one or more atoms of ring D act as electron acceptors, they must employ the first upper vacant MO localized on them.

Conformational aspects.

The most active molecules belong to group B, all having ring D. As the O-phenyl group has much conformational freedom we should expect that, if a group of molecules exist in zones II and III of the space around the receptor, we shall have a distribution of conformations. Now, if we examine molecules 43 and 44, the most active ones of the whole series, we may notice at once that the substituents placed on ring C limit the conformational freedom of the O-phenyl moiety. Fig. 13 shows the superimposition of the heavy-atom skeletons of molecules 43 and 44 [84].

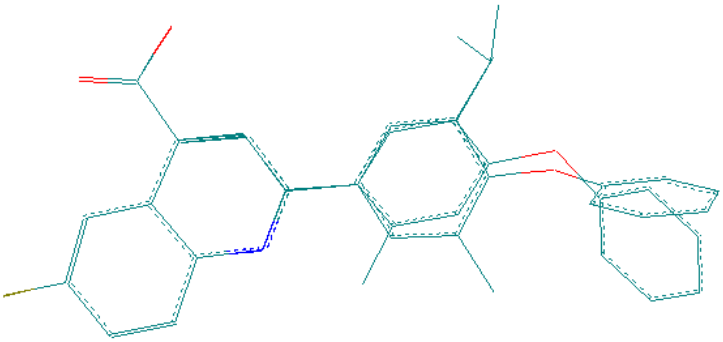

Figure 13. Superimposition of the heavy-atom skeleton of molecules 43 and 44

Then, if the molecules interact with an extra site using ring D (see below), a promising way to improve their activity is by exploring substitutions on ring C with alkyl groups to find the combination that will most correctly hinder the conformational freedom of the O-phenyl moiety. The use of other kinds of substituents will probably alter the electronic structure of the COOH-ring A-ring B system. This result is in complete agreement with the suggestion of de Brabander et al. [40]. Changes in the electronic structure should only be explored (for example a combination of molecules 42 and 44) after determining the optimal conformation of the O-phenyl group.

Electronic structure and inhibition of VSV replication in group A of molecules.

For group A of molecules, a variable-by-variable (VbV) analysis shows that a high inhibitory capacity of VSV replication is related to a high value of $F_{16}(LUMO+1)^*$ and a low value of $F_3(LUMO+2)^*$. The variation of the inhibitory capacity is orbital-controlled. Atoms 3 and 16 belong, respectively, to rings A and C (see Fig. 3). Considering that $LUMO_{16}$* and $(LUMO+1)_{16}$* have π nature, we suggest that atom 16 is acting as an electron-acceptor center through its two lowest vacant local MOs. In the case of atom 3, its LUMO* and (LUMO+1)* are of π nature. A coherent suggestion is that atom 3 also acts as an electron-acceptor center through the two lowest vacant local MOs. Fig. 14 presents the corresponding partial two-dimensional (2D) inhibitory pharmacophore.

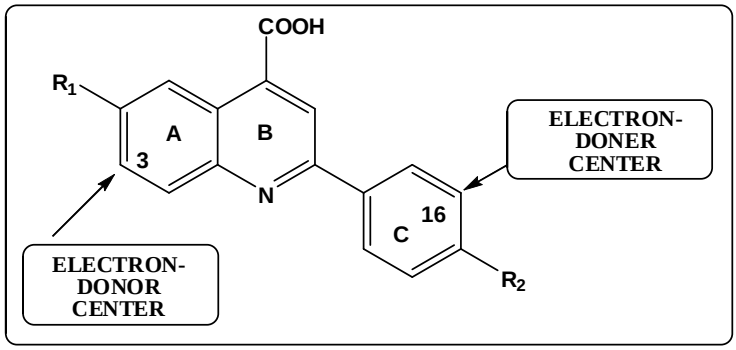

Figure 14. Partial 2D anti-VSV replication pharmacophore for group A

Electronic structure and inhibition of VSV replication in group B of molecules.

The results for group B are more complex. First of all, Table 6 shows that there are no significant correlations among independent variables. Table 5 indicates that the importance of the variables is $S_{17}^{E}(HOMO-1)^{*}$ > μ_{19} > $F_{18}(HOMO-1)^{*}$ > $F_{13}(LUMO+1)^{*}$ = $S_{22}^{N}(LUMO+2)^{*}$ > $F_{19}(LUMO+1)^{*}$ > $F_{15}(HOMO-1)^{*}$. A VbV analysis of Eq. 3 indicates that a high inhibitory capacity for VSV replication is associated with low values for $S_{17}^{E}(HOMO-1)^{*}$, μ_{19}, $F_{19}(LUMO+1)^{*}$ and $S_{22}^{N}(LUMO+2)^{*}$; and with high values for $F_{18}(HOMO-1)^{*}$, $F_{13}(LUMO+1)^{*}$, $F_{15}(HOMO-1)^{*}$. As in the case of Eq. 1, the variation of the inhibitory replication capacity is orbital-controlled [85]. The fundamental reason for this fact is that living beings are the result of hundreds of millions of years of evolution. During that time recognition mechanisms have become very specific and complex to protect the organisms from their chemical environment. Otherwise, any new molecule appearing may disrupt the chemical/biochemical processes of the host and kill it. Table 7 presents the detailed local molecular orbital structure of atoms 17-19 (see Fig. 3, Nomenclature: Molecule (HOMO) / (HOMO-2)* (HOMO-1)* (HOMO)*-(LUMO)* (LUMO+1)* (LUMO+2)*)).

Table 7. Local Molecular Orbital Structure of Atoms 17-19

Mol.	Atom 17 (C)	Atom 18 (=O)	Atom 19 (-O-)
17 (97)	86π90σ92σ-98π99π100π	92π93π96π-98π99π100π	88π90σ92n-98π101π106π
18 (93)	85π86σ88σ-94π95π96π	88π89π92π-94π95π97π	86σ88n89n-94π97π101π
19 (106)	96π98σ100σ-107π108π110π	101π102π105π-107π108π110π	98n100n101n-107π110π115π
20 (109)	101π102σ104σ-110π111π112π	104π105π108π-110π111π112π	101π102n104n-110π112π113π
21 (97)	87π88π90σ-98π99π101π	90π95π96π-98π99π101π	87π88π90n-98π101π105π
22 (100)	89π92σ95σ-101π102π104π	95π96π98π-101π102π104π	92n95n98π-101π102π104π
23 (105)	97π98σ100σ-106π107π108π	98π103π104π-106π107π108π	96π97π98n-106π108π113π
24 (89)	81π82σ85σ-90π91π93π	85π86π88π-90π91π93π	79π82n85n-90π93π97π
25 (93)	83π86σ88σ-94π95π97π	88π89π92π-94π95π97π	83π86n88n-94π97π98π
26 (93)	86σ88σ89σ-94π95π97π	88π89π92π-94π95π97π	88n89n92π-94π97π101π
27 (97)	89π90σ92σ-98π99π101π	91π92π96π-98π99π101π	89π90n92n- 98π101π105π
28 (101)	93π94σ97σ-102π103π105π	94π97π98π-102π103π105π	94n97n99π-102π105π106π
29 (104)	93π96σ101σ-105π107π109π	100π101π103π-105π107π109π	93π96n101n-105π109π113π
30 (104)	95π97σ99σ-105π106π107π	99π100π102π-105π106π108π	97n99n102π-105π108π112π
31 (97)	89π90σ92σ-98π99π100π	90π95π96π-98π100π101π	88π89π90n-98π100π101π
32 (97)	89π90σ92σ-98π99π100π	92π93π96π-98π99π100π	89π90n92n-98π100π101π
33 (97)	89π90σ93σ-98π99π101π	93π94π96π-98π99π101π	89π90n93n-98π101π105π
34 (93)	84π86σ89σ-94π95π97π	86π89π92-94π95π97π	84π86n89n-94π97π101π
35 (93)	84π85σ88σ-94π95π97π	88π89π92π-94π95π97π	85n88n89n-94π97π101π
37 (97)	89σ90σ91σ-98π99π100π	92π94π96π-98π99π100π	88π89n90n-98π100π105σ
38 (96)	88π89σ91σ-97π98π99π	91π94π95π-97π100π103π	86π87π89n-97π100π104σ
39 (97)	89π90σ92σ-98π99π100π	92π93π96π-98π99π100π	90n92n96π-98π100π105π
40 (101)	93π94σ96σ-102π103π104π	94π96π97π-102π103π104π	94n96n98π-102π104π109π
41 (106)	97π98σ101σ-107π108π111π	100π101π102π-107π108π111π	97π98n101n-107π111π115π
42 (109)	101π102σ104σ-110π111π112π	104π105π107π-110π111π112π	102n104n107π-110π113π117π
43 (101)	93π94σ96σ-102π103π104π	94π96π98π-102π103π104π	94n96n98π-102π104π109π
44 (109)	101π102σ104σ-110π112π116π	101π102π104π-110π112π117π	101π102n104n-110π112π117π

We can see that $S_{17}^{E}(HOMO-1)^{*}$ and $(HOMO-1)_{17}$* are of σ nature. A low value for $S_{17}^{E}(HOMO-1)^{*}$ can be obtained by reducing the corresponding Fukui index, by lowering the corresponding MO eigenvalue or by both procedures. If we consider that this σ MO has a non-deformable electron density (in comparison with π MOs), and that it is located very far from the molecular HOMO, we suggest that a low electron density of this MO favors the approach of an occupied π MO that is acting as an electron donor.

A low value for μ_{19} (atom 19 is the OH oxygen), which is a negative number, suggests that the $HOMO_{19}$*-$LUMO_{19}$* mid-point should be shifted to lower energies for an optimal activity. This is in agreement with the fact that $HOMO_{19}$* is located well below the molecular HOMO. This, in turn, indicates that atom 19 is not acting as an electron donor. Now, if it acts as an electron-acceptor center, it is probably through an H-bond with a less electronegative atom of the partner (for example, nitrogen or sulphur). A small value of $F_{19}(LUMO+1)^{*}$ (a π MO) indicates that only $(LUMO)_{19}$* participates in this interaction. Note from Table 7 that in only one case $(LUMO+1)_{19}$* coincides with the molecular (LUMO+1). A high value for $F_{18}(HOMO-1)^{*}$ (a π MO), together with the fact that $(HOMO)_{18}$* is also a π MO, indicates that atom 18 acts as an electron donor through its two

highest occupied local MOs. These results and interpretations are in agreement with the fact that the COOH moiety is totally necessary for the inhibitory capacity of VSV replication to be manifest. Now, considering atoms 17-19 together, it also possible to suggest that they might be involved in a π-π stacking-like interaction. The method used here is unable to distinguish between these two possibilities. When the COOH moiety is coplanar with the aromatic ring it can adopt only two conformations, one rotated by 180◦ with respect to the other. In the fully optimized geometries, in some cases the COOH group adopts one conformation and in others the other. The internal rotation barrier of the ring-COOH system is low, allowing both conformations. We cannot assert with certainty what the exact orientation of the COOH group is during its interaction with a partner. In fact, the only important datum is the initial COOH orientation in the molecules when they are added to the biological system to measure their inhibitory effect. In the case of molecule 37, the COOH and the aromatic moieties are not coplanar due to the introduction of a methyl group. In molecule 38 the CH_2 linking atoms 8 and 12 also breaks the aromatic-COOH coplanarity. A high value for $F_{13}(LUMO+1)^*$, a π MO, indicates that this atom acts as an electron-acceptor center, through $LUMO_{13}$* and $(LUMO+1)_{13}$*. A high value for $F_{15}(HOMO-1)^*$ indicates that atom 15 acts as an electron donor through $HOMO_{15}$* and $(HOMO-1)_{15}$*. Given the proximity of atoms 13 and 15, and that they belong to the same conjugated system, it is possible that both participate in a π-π stacking interaction with the partner. A low value for $S_{22}^{N}(LUMO+2)^*$ (a π MO) suggests that atom 22 is acting as an electron acceptor but only through $LUMO_{22}$*. All these suggestions are depicted in the two-dimensional (2D) partial inhibition pharmacophore shown in Fig. 15. The appearance of atom 22 is a good demonstration that ring D (see Fig. 3) is interacting with an extra site that is unavailable to group A of molecules. Note that the pharmacophores for groups A and B do not show incompatible elements between them.

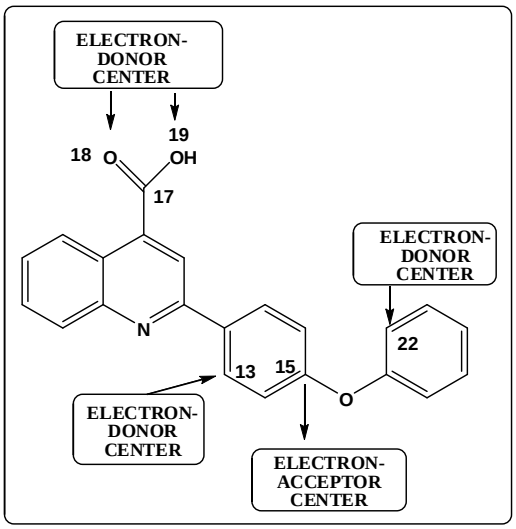

Figure 15. Partial 2D anti-VSV replication pharmacophore for group B

CONCLUSION

High quality relationships between electronic structure and inhibition of VSV replication have been obtained for a group of 4-quinolinecarboxylic acid analogues. The inhibitory capacity is orbital-controlled. One group of molecules seems to interact with an additional site. Suggestions are made to improve the inhibitory potency.

Acknowledgements
Prof. Dr. Bruce K. Cassels (Faculty of Sciences, University of Chile) is gratefully acknowledged for helpful comments.

REFERENCES

[1] RW Simpson; RE Hauser, *Virol.*, **1966**, 29, 654-667.

[2] J Huppert; M Rosenbergova; L Gresland; L Harel, "Properties of RNA from Vesicular Stomatitis Virus," in *The Molecular Biology of Viruses*, J. S. Colter, and W. Paranchych Eds., pp. 463-468, Academic Press, **1967**.
[3] T Nakai; AF Howatson, *Virol.*, **1968**, 35, 268-281.
[4] M Soria; SP Little; AS Huang, *Virol.*, **1974**, 61, 270-280.
[5] GH Weber; JE Dahlberg; M Cottler-Fox; U Heine, *Virol.*, **1974**, 62, 284-287.
[6] LA Ball; CN White, *Proc. Natl. Acad. Sci USA*, **1976**, 73, 442-446.
[7] A Gordon; AK Banerjee, *Proc. Natl. Acad. Sci USA*, **1976**, 73, 1504-1508.
[8] J Orenstein; L Johnson; E Shelton; RA Lazzarini, *Virol.*, **1976**, 71, 291-301.
[9] NF Moore; EJ Patzer; RR Wagner; PL Yeagle; WC Hutton; RB Martin, *Bioch. Biophy. Acta. Biomemb.*, **1977**, 464, 234-244.
[10] DJ McGeoch; NT Turnbull, *Nucl. Ac. Res.*, **1978**, 5, 4007-4024.
[11] BL Semler; J Perrault; JJ Holland, *Nucl. Ac. Res.*, **1979**, 6, 3923-3934.
[12] K Ghosh; HP Ghosh, *Nucl. Ac. Res.*, **1982**, 10, 6341-6351.
[13] AK Banerjee; DS Gill; PS Masters, *Virus Res.*, **1985**, 3, Supplement 1, 47.
[14] AK Banerjee; D Chattopadhyay, "Structure and Function of the RNA Polymerase of Vesicular Stomatitis Virus," in *Advances in Virus Research*, F. A. M. Karl Maramorosch, and S. Aaron J Eds., vol. 38, pp. 99-124, Academic Press, **1990**.
[15] A Barge; J Gagnon; A Chaffotte; P Timmins; J Langowski, et al., *Virol.*, **1996**, 219, 465-470.
[16] Y Gaudin; J Sturgis; M Doumith; A Barge; B Robert; RWH Ruigrok, *J. Mol. Biol.*, **1997**, 274, 816-825.
[17] F Iseni; R Eacute; F Baudin; D Blondel; RWH Ruigrok, *RNA*, **2000**, 6, 270-281.
[18] M Gaudier; Y Gaudin; M Knossow, *EMBO J.*, **2002**, 21, 2886-2892.
[19] H Ding; TJ Green; M Luo, *Acta Cryst. D*, **2004**, 60, 2087-2090.
[20] TJ Green; M Luo, *Acta Cryst. D*, **2006**, 62, 498-504.
[21] TJ Green; X Zhang; GW Wertz; M Luo, *Science*, **2006**, 313, 357-360.
[22] AA Rahmeh; AD Schenk; EI Danek; PJ Kranzusch; B Liang, et al., *Proc. Natl. Acad. Sci USA*, **2010**, 107, 20075-20080.
[23] C Leyrat; R Schneider; EA Ribeiro Jr; F Yabukarski; M Yao, et al., *J. Mol. Biol.*, **2012**, 423, 182-197.
[24] PK Olitsky; HR Cox; JT Syverton, *Science*, **1933**, 77, 611-612.
[25] RJ Blattner, *J. Pediat.*, **1951**, 38, 141-142.
[26] J Bloom, *Or. Surg. Or. Med. Or. Pathol.*, **1951**, 4, 515.
[27] DH Ferris; RP Hanson; RJ Dicke; RH Roberts, *J. Infect. Dis.*, **1955**, 96, 184-192.
[28] HH Skinner, *J. Comp. Pathol. Ther.*, **1957**, 67, 87-105.
[29] HH Skinner, *J. Comp. Pathol. Ther.*, **1957**, 67, 69-86.
[30] L Karstad; J Spalatin; RP Hanson, *J. Infect. Dis.*, **1959**, 105, 188-195.
[31] M Mussgay; O Suárez, *Virol.*, **1962**, 17, 202-204.
[32] GH Bergold; OM Suárez; K Munz, *J. Inv. Pathol.*, **1968**, 11, 406-428.
[33] W Levinson; H Oppermann; P Rubenstein; J Jackson, *Virol.*, **1978**, 85, 612-616.
[34] DN Yarde; RA Nace; SJ Russell, *Exp. Hematol.*, **2013**, 41, 1038-1049.
[35] RW Randle; SA Northrup; SJ Sirintrapun; DS Lyles; JH Stewart Iv, *Surgery*, **2013**, 154, 1323-1330.
[36] M Moerdyk-Schauwecker; NR Shah; AM Murphy; E Hastie; P Mukherjee; VZ Grdzelishvili, *Virol.*, **2013**, 436, 221-234.
[37] MJ Atherton; BD Lichty, *Immunother.*, **2013**, 5, 1191-1206.
[38] F Le Boeuf; N Niknejad; J Wang; R Auer; JI Weberpals, et al., *Int. J. Canc.*, **2012**, 131, E204-E215.
[39] G Chang; S Xu; M Watanabe; HR Jayakar; MA Whitt; JR Gingrich, *J. Urol.*, **2010**, 183, 1611-1618.
[40] P Das; X Deng; L Zhang; MG Roth; BMA Fontoura, et al., *ACS Med. Chem. Lett.*, **2013**, 4, 517-521.
[41] YC Martin, *Quantitative drug design: a critical introduction*, M. Dekker, New York, **1978**.
[42] JS Gómez-Jeria, *Int. J. Quant. Chem.*, **1983**, 23, 1969-1972.
[43] JS Gómez-Jeria, "Modeling the Drug-Receptor Interaction in Quantum Pharmacology," in *Molecules in Physics, Chemistry, and Biology*, J. Maruani Ed., vol. 4, pp. 215-231, Springer Netherlands, **1989**.
[44] JS Gómez-Jeria; M Ojeda-Vergara; C Donoso-Espinoza, *Mol. Engn.*, **1995**, 5, 391-401.
[45] JS Gómez-Jeria; M Ojeda-Vergara, *J. Chil. Chem. Soc.*, **2003**, 48, 119-124.
[46] JS Gómez-Jeria, *Elements of Molecular Electronic Pharmacology (in Spanish)*, Ediciones Sokar, Santiago de Chile, **2013**.
[47] JS Gómez-Jeria, *Canad. Chem. Trans.*, **2013**, 1, 25-55.
[48] RS Mulliken, *J. Chem. Phys.*, **1955**, 23, 1833-1840.

[49] K Fukui; H Fujimoto, *Frontier orbitals and reaction paths: selected papers of Kenichi Fukui*, World Scientific, Singapore; River Edge, N.J., **1997**.
[50] JS Gómez-Jeria; D Morales-Lagos, "The mode of binding of phenylalkylamines to the Serotonergic Receptor," in *QSAR in design of Bioactive Drugs*, M. Kuchar Ed., pp. 145-173, Prous, J.R., Barcelona, Spain, **1984**.
[51] JS Gómez-Jeria; DR Morales-Lagos, *J. Pharm. Sci.*, **1984**, 73, 1725-1728.
[52] JS Gómez-Jeria; D Morales-Lagos; JI Rodriguez-Gatica; JC Saavedra-Aguilar, *Int. J. Quant. Chem.*, **1985**, 28, 421-428.
[53] JS Gómez-Jeria; D Morales-Lagos; BK Cassels; JC Saavedra-Aguilar, *Quant. Struct.-Relat.*, **1986**, 5, 153-157.
[54] JS Gómez-Jeria; BK Cassels; JC Saavedra-Aguilar, *Eur. J. Med. Chem.*, **1987**, 22, 433-437.
[55] JS Gómez-Jeria; M Ojeda-Vergara, *Int. J. Quant. Chem.*, **1997**, 61, 997-1002.
[56] JS Gómez-Jeria; L Lagos-Arancibia, *Int. J. Quant. Chem.*, **1999**, 71, 505-511.
[57] JS Gómez-Jeria; L Lagos-Arancibia; E Sobarzo-Sánchez, *Bol. Soc. Chil. Quím.*, **2003**, 48, 61-66.
[58] JS Gómez-Jeria; F Soto-Morales; G Larenas-Gutierrez, *Ir. Int. J. Sci.*, **2003**, 4, 151-164.
[59] JS Gómez-Jeria; LA Gerli-Candia; SM Hurtado, *J. Chil. Chem. Soc.*, **2004**, 49, 307-312.
[60] F Soto-Morales; JS Gómez-Jeria, *J. Chil. Chem. Soc.*, **2007**, 52, 1214-1219.
[61] JS Gómez-Jeria; F Soto-Morales; J Rivas; A Sotomayor, *J. Chil. Chem. Soc.*, **2008**, 53, 1393-1399.
[62] JS Gómez-Jeria, *J. Chil. Chem. Soc.*, **2010**, 55, 381-384.
[63] C Barahona-Urbina; S Nuñez-Gonzalez; JS Gómez-Jeria, *J. Chil. Chem. Soc.*, **2012**, 57, 1497-1503.
[64] T Bruna-Larenas; JS Gómez-Jeria, *Int. J. Med. Chem.*, **2012**, 2012 Article ID 682495, 1-16.
[65] DA Alarcón; F Gatica-Díaz; JS Gómez-Jeria, *J. Chil. Chem. Soc.*, **2013**, 58, 1651-1659.
[66] JS Gómez-Jeria; M Flores-Catalán, *Canad. Chem. Trans.*, **2013**, 1, 215-237.
[67] A Paz de la Vega; DA Alarcón; JS Gómez-Jeria, *J. Chil. Chem. Soc.*, **2013**, 58, 1842-1851.
[68] I Reyes-Díaz; JS Gómez-Jeria, *J. Comput. Methods Drug Des.*, **2013**, 3, 11-21.
[69] JS Gómez-Jeria, *Int. Res. J. Pure App. Chem.*, **2014**, 4, 270-291.
[70] JS Gómez-Jeria, *Der Pharm. Lett.*, **2014**, 6., 95-104.
[71] JS Gómez-Jeria, *Brit. Microbiol. Res. J.*, **2014**, In press.,
[72] JS Gómez-Jeria, *SOP Trans. Phys. Chem.*, **2014**, In press,
[73] D Muñoz-Gacitúa; JS Gómez-Jeria, *J. Comput. Methods Drug Des.*, **2014**, 4, 33-47.
[74] D Muñoz-Gacitúa; JS Gómez-Jeria, *J. Comput. Methods Drug Des.*, **2014**, 4, 48-63.
[75] DI Pino-Ramírez; JS Gómez-Jeria, *Amer. Chem. Sci.*, **2014**, 4, 554-575.
[76] F Salgado-Valdés; JS Gómez-Jeria, *J. Quant. Chem.*, **2014**, 2014 Article ID 431432, 1-15.
[77] R Solís-Gutiérrez; JS Gómez-Jeria, *Res. J. Pharmac. Biol. Chem. Sci.*, **2014**, 5, 1401-1416.
[78] MJ Frisch; GW Trucks; HB Schlegel; GE Scuseria; MA Robb, et al., Gaussian98 Rev. A.11.3, Gaussian, Pittsburgh, PA, USA, **2002**.
[79] JS Gómez-Jeria, D-Cent-QSAR: A program to generate Local Atomic Reactivity Indices from Gaussian log files. 1.0, Santiago, Chile, **2014**.
[80] JS Gómez-Jeria, *J. Chil. Chem. Soc.*, **2009**, 54, 482-485.
[81] Statsoft, Statistica 8.0, 2300 East 14 th St. Tulsa, OK 74104, USA, **1984-2007**.
[82] RD Dennington; TA Keith; JM Millam, GaussViev 5.0.8, 340 Quinnipiac St., Bldg. 40, Wallingford, CT 06492, USA, **2000-2008.**
[83] U Varetto, Molekel 5.4.0.8, Swiss National Supercomputing Centre: Lugano, Switzerland, **2008**.
[84] Hypercube, Hyperchem 7.01, 419 Phillip St., Waterloo, Ontario, Canada, **2002**.
[85] G Klopman, *J. Am. Chem. Soc.*, **1968**, 90, 223-234.